ISSN 1063-4576, Journal of Superhard Materials, 2021, Vol. 43, No. 6, pp. 379–391. © Allerton Press, Inc., 2021.
Ukrainian Text © The Author(s), 2021, published in Nadtverdi Materialy, 2021, Vol. 43, No. 6, pp. 3–17.

Shear-Induced Metallization on the (001) and (111) Faces of Diamond during Hardness Tests

S. N. Dub[a], *, A. S. Nikolenko[b], P. M. Lytvyn[b], S. O. Ivakhnenko[a], V. V. Strelchuk[b], O. M. Suprun[a], V. V. Lysakovskii[a], and I. M. Danilenko[b]

[a] *Bakul' Institute for Superhard Materials, National Academy of Sciences of Ukraine, Kyiv, 04074 Ukraine*
[b] *Lashkaryov Institute of Semiconductor Physics, National Academy of Sciences of Ukraine, Kyiv, 01030 Ukraine*
**e-mail: lz@ism.kiev.ua*

Received June 17, 2021; revised July 25, 2021; accepted August 1, 2021

Abstract—For the first time, shear-induced metallization on the (001) face of diamond single crystals of types Ib, IIa and IIb during hardness tests is studied. The tests are performed using the Vickers and Berkovich indenters on diamond single crystals grown by the temperature gradient method. In the Raman spectra of imprints obtained on the (001) face of diamond, intense photoluminescence bands with a complex shape are found, which complicates the identification of the phonon bands of the sp^2 phase of carbon. The sp^2 phase of carbon in the imprints on the (001) face is reliably revealed only for diamonds of type IIb and only in the case of using the Berkovich indenter. It is found that graphitization during hardness tests on the (001) face of diamond of type IIb is much less than on the (111) face. The recorded photoluminescence with a maximum at about 510 nm can be considered as evidence of the formation of the mixed sp^2/sp^3 phase of amorphous carbon in the imprints on the (001) face of diamond in the initial stages of graphitization.

Keywords: diamond, hardness, Mott transition, diamond metallization, Raman spectroscopy

DOI: 10.3103/S1063457621060034

INTRODUCTION

It is known that the bandgap between the valence and conductivity bands decreases when an external pressure is applied to a dielectric material. With some critical pressure, the valence band overlaps with the conduction band and the dielectric becomes a conductor. This effect is known as the Mott transition [1, 2]. Typically, this pressure is much higher than the pressure created when measuring the hardness of the material and the Mott transition is not observed during the hardness test. For example, the hardness of gallium arsenide is about 7 GPa and the high pressure metallic phase is formed only under a pressure of 16 GPa [3], so the high pressure phase is not formed upon the indentation of GaAs during the hardness test [4]. But there are exceptions for single crystals of silicon and germanium with an open shell structure and strictly directed covalent bonds. For these materials, the pressure created under the indenter during the hardness test is sufficient for the disappearance of the bandgap and the formation of a high pressure plastic metallic phase at the place of contact [5–8]. It was found that ordinary silicon Si-I with a diamond lattice is converted under the indenter into the high pressure Si-II phase with a lattice of β tin. During the phase transformation in the silicon lattice, the angles between the atomic bonds change and the lengths of the bonds change slightly (Fig. 1). Under this condition, the volume of the material is reduced by about 20% (the material in the imprint is compacted). During unloading of the indenter, the metallic phase of high pressure Si-II in the imprint is converted, depending on the test conditions, either into amorphous silicon a-Si or into a mixture of metastable crystalline phases of Si-XII and Si-III with an increase in the volume of the material in the imprint (sealing) [9]. The occurrence of phase transformations in silicon during the hardness test is confirmed by the following data: measurement of the electrical resistivity in the region of contact [5, 10]; extrusion of high pressure plastic metallic phase from the imprint [6]; data of structural studies (electron diffraction and TEM [11], and microRaman spectroscopy [7]); features of the temperature dependence of the hardnes [12]; nanoindentation data (formation of a wide hysteresis loop as a result of compression/decompression of the material in the region of contact as a result of an increase and a decrease in the pressure under the indenter) [4, 13]. The fact of metallization of Si in the imprint is indirectly confirmed by the data obtained when studying the effect of hydrostatic compression on silicon

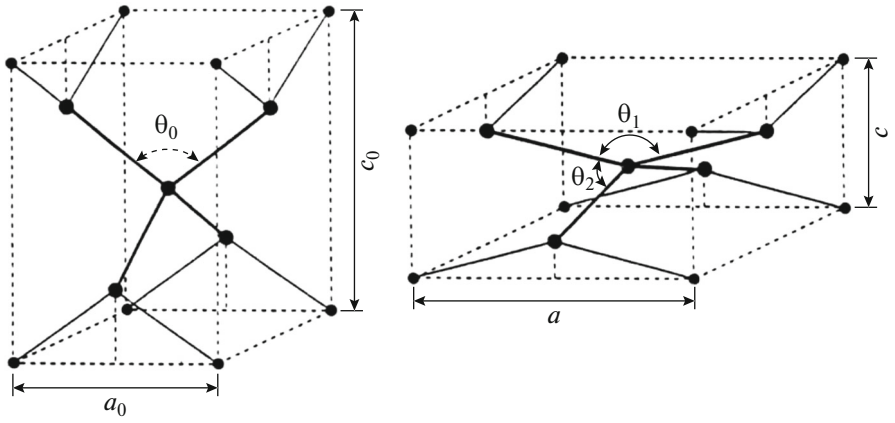

Fig. 1. Conversion of the diamond structure into the tetragonal structure of β-tin during compression of diamond along the four fold symmetry axis [2].

[14]. Namely, the hardness of silicon (about 12 GPa), which is equal to the average contact pressure during the indentation, coincides with the pressure required to convert a brittle semiconductor with a diamond lattice (Si-I) into a plastic conductor with a lattice of β-tin (Si-II), i.e., 11.56 GPa.

Diamond has the same type of crystal lattice as silicon and germanium do. Therefore, it can be expected that the contact pressure during the diamond hardness test will be sufficient for the formation of the high pressure metallic phase of carbon [15, 16]. Gogotsi and Domnich first recorded Raman scattering spectra of hardness test imprints on the (111) face of diamond [17, 18]. They detected disordered graphite in the imprint. Since diamond is stable under high pressures and graphite is metastable, a direct diamond–graphite phase transition cannot occur under a load. It is likely that sufficient pressures/shear stresses develop in the region of contact during the diamond hardness test to form a metastable high pressure metallic phase of carbon, which is converted to graphite with a subsequent decrease in the pressure. Grigor'ev observed a decrease in the resistivity of the diamond in the imprint under a load and the return of the resistivity to the initial value after unloading the indenter [19]. That is, the results of measuring the resistivity of the imprint on the diamond surface confirms the assumption about the formation of a metallic phase of carbon in the region of contact of the diamond indenter with the surface of the diamond.

A further evidence of diamond metallization was obtained when studying the elastic deformation of diamond nanopillars or nanoneedles with a diameter of about 200 nm [20]. It turned out that diamond nanpillars can be elastically deformed by 12% during bending. Such elastic deformations turned out to be enough to overlap the bandgap, so metallization took place in the deformed region of the pillar [21]. Moreover, shear metallization of diamond during the elastic deformation of the pillar is reversible in contrast to hardness tests, in which the metallization is irreversible (graphitization). That is, the elastic deformation can adjust the bandgap width in diamond [22]. Though the fact of diamond metallization during its deformation is not in doubt, but the effect is still poorly understood.

Previously, single crystals of synthetic diamond of type Ib were prepared by spontaneous crystallization from a supersaturated solution of carbon in metal solvents. The typical synthesis time is 1–2 min, and the crystal size is <1 mm. Such crystals are of low quality, namely, the samples contain many paramagnetic nitrogen sites of type C and metal inclusions from the solvent, and they are characterized by a high density of growth dislocations (Fig. 2). Such crystals are quite suitable for the production of diamond tools. If large diamond crystals are required, which are of high quality both in composition and structure, then the temperature gradient method is used [23]. In this case, the synthesis of diamonds takes several days, during which crystals a few millimeters in size with a low density of dislocations are grown [24]. It is possible to synthesize diamond single crystals of type IIa with a low density of dislocations and a low content of nitrogen sites. Natural diamonds of this type do not exist, since they have either a low density of dislocations, but high content of nitrogen sites unevenly distributed over the volume of the sample (type Ia) or they are crystals with low nitrogen content, but with a high density of dislocations (type IIa). Additional doping of the growth systems with boron allows one to synthesize diamond single crystals that have semiconductor properties (type IIb) [25, 26]. Such crystals have a blue color, the intensity of which varies from light blue to dark blue, depending on the concentration of boron.

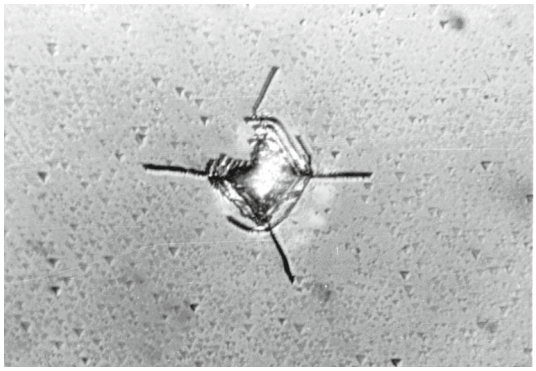

Fig. 2. Imprint of the Vickers indenter on the (111) face of diamond of type Ib synthesized by spontaneous crystallization; one of the diagonals is parallel to the ⟨011⟩ direction, the other one (perpendicular to the basis of the drawing) is parallel to the ⟨112⟩ direction; ring and radial cracks can be seen in the ⟨011⟩ directions on the {111} planes.

To study shear metallization observed earlier during the hardness test of diamond, only the hardest (111) faces and only the Vickers indenter were used. Natural diamonds and diamonds synthesized by spontaneous crystallization were tested [17, 18, 27]. In this work, the phase composition of the material in the imprints on the (001) and (111) faces of diamond single crystals of types Ib, IIa, and IIb, which are synthesized by the temperature gradient method, is studied for the first time by confocal Raman spectroscopy. It is found that strong luminescence of the imprints on the (001) face of diamond makes it difficult to obtain graphite bands in the microRaman spectrum. Graphite bands were possible to obtain only for the Berkovich imprints on the (001) face of diamond of type IIb.

EXPERIMENTAL

Synthetic diamond single crystals of types Ib, IIa, and IIb were used for the experiments, which were prepared at a temperature of 1420–1500°C and a pressure of 5.7–6.1 GPa with a growth rate of 1–2 mg/h. Diamonds were grown using a high pressure device of the toroid type by the temperature gradient method [28]. The obtained diamond crystals of cubic octahedral habit were 3–5 mm in dimensions and 0.075–0.13 carats in weight.

Room temperature hardness tests were performed on a PMT-3 microhardness testing machine with Vickers and Berkovich indenters under a load of 500 g. Imprints were made on the (001) and (111) faces. On the (001) face, the diagonals of the Vickers indenter were parallel to the ⟨011⟩ directions and, for the Berkovich indenter, one of the imprint edges was parallel to the ⟨011⟩ direction. On the (111) face, the edges of the Berkovich imprint were parallel to the ⟨011⟩ directions and, for the Vickers imprint, one of the diagonals was parallel to the ⟨011⟩ direction and the second one was parallel to the ⟨112⟩ direction (see Fig. 2).

The Berkovich hardness (ratio of the load to the surface area of the imprint side) is equal to $H_B = 1570P/l^2$, where P is the load in N, l is the height of the imprint in μm [29]. For the Vickers indenter, $H_B = 1854P/d^2$, where d is the diagonal of the imprint. Pyramidal indenters give similar imprints, so the average deformation in the region of contact at the stage of developed plasticity does not depend on the load and is determined by the geometry of the indenter. The average deformation is about 7% for the Vickers indenter [30] and about 9% for the Berkovich indenter. That is, the Berkovich indenter creates a higher strain in the region of contact, so diamond metallization in the region of contact with it can be stronger than in the region of contact with the Vickers indenter.

Three-dimensional topometric measurements of the shape of the indenter imprint on the surface of diamond single crystals were performed with a NanoScope IIIa scanning probe microscope of series Dimension 3000TM. The method of atomic force microscopy (AFM) in the periodic contact mode (Tapping-ModeTM) was used for measurements. During the measurements, silicon probes with a nominal tip radius of 5–10 nm were used, which guaranteed a lateral resolution of 1 nm and a vertical resolution of about 0.05 nm.

Raman spectra were measured at room temperature in the backscattering geometry using a Horiba Jobin-Yvon T-64000 triple Raman spectrometer (Horiba Scientific, Villeneuve d'Ascq, France) equipped with an electrically cooled CCD detector and an Olympus BX41 confocal microscope. An Ar/Kr ion laser line with a wavelength of 488 nm was used to excite Raman scattering. Using a 100x/NA 0.9 microlens,

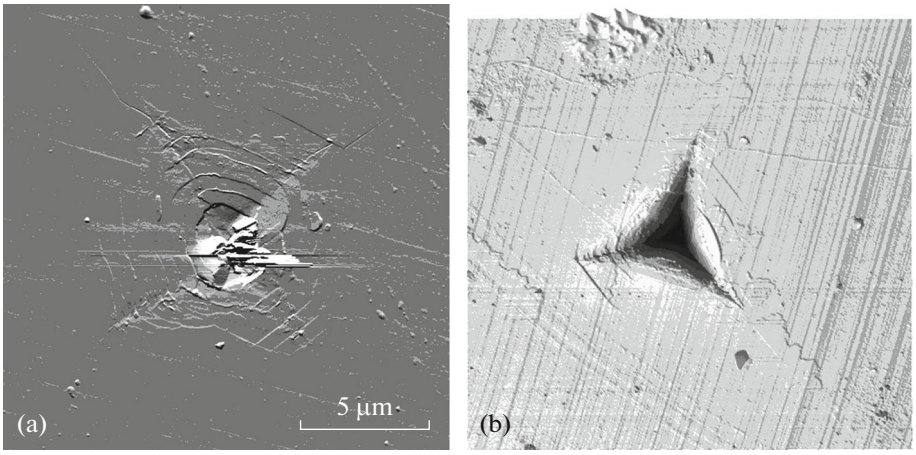

Fig. 3. AFM images of the imprints created by the (a) Vickers and (b) Berkovych indenters on the (111) face of diamonds of type Ib synthesized by the temperature gradient method.

the laser radiation was focused on the surface of the sample in a spot with a diameter of about 0.6 μm. MicroRaman mapping of hardness imprints on the diamond surface was performed using a piezo-controlled *XYZ* scanning table, which enables automatic scanning of the sample with a step of 0.1 μm. To increase the spatial resolution, a 100 μm confocal diaphragm was used, which was placed in the focal plane of the microscope.

RESULTS

Hardness of Diamonds Synthesized by the Temperature Gradient Method

Atomic force microscopy images of Berkovich and Vickers imprints on the (111) face of diamonds of type Ib are shown in Fig. 3. It is seen that the measurement of the size of the imprints on the diamond surface is complicated by the formation of radial cracks from the corners of the imprint and the strong concavity of the imprint sides inward. As a result, it is difficult to determine where the imprint ends and the radial crack begins (see Fig. 3). Therefore, the accuracy of measuring the size of the imprints is low. However, the boundaries of the imprint on the diamond surface are more clearly visible for the Berkovich indenter and we further analyzed only the results of measuring the hardness of diamond with the Berkovich indenter.

As noted above, the Berkovich hardness is found as the ratio of load P (N) to the area of the side surface of the imprint by the following standard equation:

$$H_{\text{B}} = \frac{\sqrt{3}\sin\varphi_i}{l^2} P = 1570\frac{P}{l^2}, \quad (1)$$

where l is the average height of the imprint in μm, and the φ_i angle equals 65.3°. To apply this equation, two assumptions are made. First, the proportionality factor in equation (1) is determined only by the geometry of the indenter and it is assumed by default that it does not depend on the properties of the sample material. That is, it is assumed that the elastic deformation of the diamond indenter during the hardness test can be neglected (rigid indenter). This assumption is valid when testing metals whose elastic modulus is much lower than the elastic modulus of diamond from which the Berkovich indenter is made. But to test high modulus materials, such as diamond and cBN, it is necessary to take into account the change in the geometry of the indenter due to its elastic deformation when determining the hardness values. In this study, the changes in the geometry of the pyramidal indenter are taken into account using the equation obtained by Galanov et al. [31]:

$$\cot\varphi = \cot\varphi_i - \frac{2HM}{E^*}, \quad (2)$$

where φ is the angle of the indenter under a load, HM is the Meyer hardness of the sample, and E^* is the reduced elastic modulus. The results of determining the coefficient of proportionality $\sqrt{3}\sin\varphi$ in equation (1) for materials with different hardnesses and elastic moduli are given in Table 1.

Table 1. Effect of the elastic deformation of the Berkovich indenter on its geometry for materials with different elastic moduli

Sample	E, GPa	Poisson's ratio	HM, GPa	$2HM/E^*$	φ, degree	$\sqrt{3}\sin\varphi$
Al	72	0.35	0.36	0.001	65.3	1.573
W	379	0.35	5.7	0.010	65.8	1.578
SiO_2	71	0.17	9	0.016	66.1	1.582
Al_2O_3	400	0.22	27	0.048	67.6	1.600
V4S	500	0.15	41	0.072	68.8	1.614
KNB	850	0.12	62	0.109	70.9	1.633
Diamond	1136	0.07	100	0.176	74.2	1.665

For an unloaded indenter, the φ_i angle is 65.3°.

Table 2. Berkovich hardness of single crystals of diamonds synthesized by the temperature gradient method under a load of 4.91 N

Diamond type	Face	Imprint height h, μm	H_B, GPa	
			1	2
Ib	(111)	9.3	105	175
IIa	(111)	8.9	116	194
IIb	(111)	9.3	105	175
IIb	(001)	9.8	95	163

Column 1 corresponds to the conventional determination of hardness according to Berkovich. Column 2 corresponds to determination of Berkovich hardness with consideration of the concavity of the imprint sides and the elastic deformation of the indenter under a load.

The geometry of the Berkovich indenter changes markedly when indenter is pressed into samples of solid and superhard materials: for diamond, the φ angle increases from 65.3° to 74.2°, but sinφ changes to a much weaker extent with an increase in the $2NM/E^*$ ratio (see Table 1). Therefore, the elastic deformation of the diamond indenter during the hardness test should be taken into account only for the hardest and high modulus materials. However, the increase in the coefficient of proportionality does not exceed 6% even in the case when a diamond single crystal is tested for hardness and equals 3.8% for cBN.

Secondly, it is assumed when applying equation (1) that the imprint on the sample surface has the shape of an equilateral triangle, and this is not always the case. For glass, annealed metals, and superhard materials, the sides of the imprint are concave (see Fig. 3). Thus, the real hardness is higher than that determined by equation (1). On the contrary, the sides of the imprint are convex for pre-deformed materials and equation (1) gives an exaggerated hardness for them [32]. To find the real contact area during the Vickers and Berkovich hardness test, we used atomic force microscopy (see Fig. 3). The results of determining the Berkovich hardness of diamond single crystals are given in Table 2.

MicroRaman Spectroscopy of Imprints on the Diamond Surface

Imprints of the Vickers and Berkovich indenters on the (001) and (111) faces of diamond single crystals of types Ib, IIa, and IIb are investigated by scanning Raman microspectroscopy. However, it is found that the recording of Raman spectra for Vickers and Berkovich imprints on the (001) face of diamond is complicated by a strong luminescent background. Reliable data on graphite formed on the (001) face are obtained only for imprints from the Berkovich indenter on diamonds of type IIb doped with boron.

Berkovich imprint on the (111) face of diamond of type IIb. In the Raman spectra recorded in the central part of the hardness test imprints on the (111) face of diamond of type IIb (Fig. 4), broad bands at frequencies of about 1350 and 1580 cm^{-1} that correspond to D and G bands of graphite disorder—which is created, probably, as a result of graphitization of diamond during indentation [18, 27]—are observed in addition to the main F_{2g} vibration band of diamond at frequencies of about 1333 cm^{-1}.

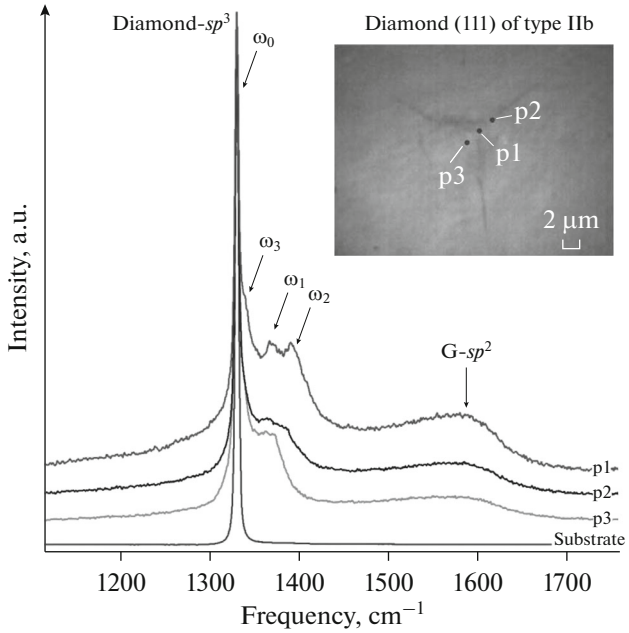

Fig. 4. Typical Raman spectra recorded in different regions of the Berkovich imprint on the (111) face of diamond of type IIb (see Fig. 3b); spectrum p1 is recorded in the center of the imprint.

In some spectra recorded in the region of imprints, a series of narrow bands with variable frequency positions denoted as ω_1, ω_2, and ω_3 are recorded on the high frequency side of the diamond band in the region 1335–1390 cm^{-1} (see Fig. 4). As previously established in [27], these lines are related to the residual compressive stresses that are formed in the region of the hardness imprint after unloading the indenter. Uniaxial or biaxial compression strains partially or completely remove the degeneracy of the triple degenerate F_{2g} band of diamond with the corresponding splitting of the Raman peak into two or three components, the positions of which undergo a gradual high frequency shift with an increase in the strain value [33]. Therefore, the bands at ω_1, ω_2, and ω_3 correspond to the components of the triplet, which appears as a result of splitting the diamond band (ω_0) under the action of uniaxial compression strains, and the observation of the more intense diamond band (ω_0) in the spectra indicates that both stressed and unstressed regions of the diamond surface fall under the laser probe at the same time. During confocal scanning at a wavelength of $\lambda_{exc} = 488$ nm, the lateral size of the laser probe is about 0.6 μm and the probing depth is about 1.8 μm.

Raman mapping of the region of hardness imprints (Fig. 5) shows an uneven spatial distribution of the sp^2 phase of carbon with its predominant localization in the center and along the edges of the imprint, which gradually decreases to the imprint edges (see Fig. 5c). Therefore, the main part of graphite formed during the hardness test of the diamond surface is concentrated in the central part of the imprint, which was exposed to the maximum pressure.

As can also be seen from Fig. 5d, the regions of residual compressive stresses in the diamond surface are preferably localized along the faces of the hardness imprint. A gradual low frequency shift of the bands at ω_1, ω_2, and ω_3 toward the diamond band at ω_0 is observed when scanning from the center of the imprint to its edge (Fig. 6), which apparently corresponds to the gradual relaxation of deformation within the investigated region. A rough estimate of the starin on the basis of the published data [33] and under the assumption of uniaxial compression in the [110] direction gives a value of about 20 GPa.

Berkovich imprint on the (001) face of diamond of type IIb. The Raman spectra of the hardness imprint on the (001) face of diamond of type IIb (Fig. 7) are generally similar to the spectra of the hardness imprint on the (111) face. In addition to the main phonon peak of the sp^3-diamond at a frequency of about 1333 cm^{-1}, differently split diamond bands (peaks ω_1, ω_2, and ω_3) and sp^2 bands of graphite disorder are also recorded in the spectra, depending on the position of the imprint. However, the D and G bands of the sp^2 graphite phase in the central part of the imprint on the (001) face are noticeably weaker than in the case of the imprint on the (111) face. The spectra of samples IIb (001) are also characterized by the presence of

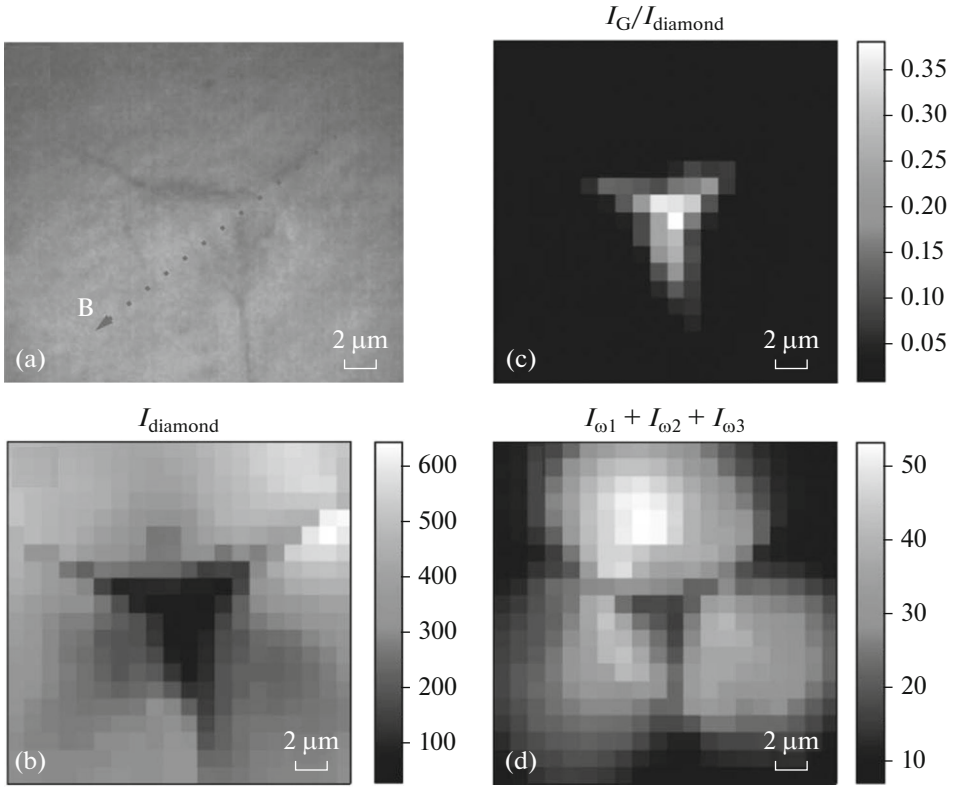

Fig. 5. (a) Optical image of a hardness test imprint on the (111) face of diamond of type IIb; (b) the distribution map of intensity $I_{diamond}$ of the Raman band of diamond at 1333 cm^{-1}; (c) ratio $I_G/I_{diamond}$ of the mean intensity values of Raman bands of graphite and diamond; (d) total intensity $I_{ω1} + I_{ω2} + I_{ω3}$ of Raman bands of strained diamond with $ω_1$, $ω_2$, and $ω_3$ in the range of 1340–1400 cm^{-1}.

a luminescent background in the region of the imprints, which prevents the clear detection of the D and G bands of the sp^2 graphite phase.

As in the previous case, the Raman spectrum (Fig. 8) shows that the sp^2 phase of graphite is localized in the center and along the edges of the hardness imprint, but the total intensity of its signal in the case of the (001) face is much lower (see Fig. 8c). Regions of residual compressive stresses in diamond are also predominantly localized along the faces of the hardness imprint (see Fig. 8d).

DISCUSSION

In this study, we used microRaman spectroscopy to investigate the hardness imprints on the (001) face of diamond for the first time. It is found that the degree of graphitization in the imprint on the (001) face of diamond is weaker than on the (111) face. This is probably due to the fact that the Vickers hardness of the (111) face of diamond is higher than the hardness of the (001) face. It is known that the deformation of diamond depends on the crystallographic orientation of the sample [21, 34]. This can also lead to weakening of graphitization in the imprints indented on the (001) face compared to the imprints indented on the (111) face.

The observed photoluminescence (PL) in the region of imprints during excitation with a wavelength of 488 nm (Fig. 9) can be caused by the radiation of both types of specific defects formed during the indentation of the (001) face of diamond and the clusters of sp^2/sp^3-carbon. It should be noted that the strongest PL signal with a maximum wavelength of about 510 nm (aproximately 2.432 eV) is recorded in the central part of the imprints, which gradually decreases to the edges of the imprint and is absent on the surface of the (001) face of diamond outside the imprint (see Fig. 9). A similar PL signal was previously observed in films of the amorphous sp^2/sp^3-carbon material [35] and amorphous carbon quantum dots with sp^2–sp^3 hybridized atomic domains [36, 37]. The increase in the PL signal intensity and the shift to the short-

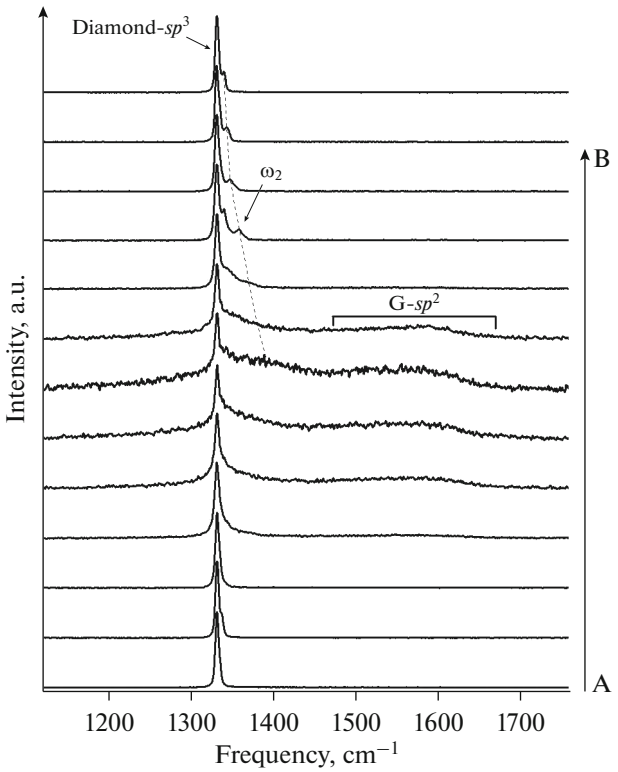

Fig. 6. Set of Raman spectra of the Berkovich imprint on the (111) face of diamond of type IIb, which are recorded along the A–B line (dashed line in Fig. 5a) and correspond to the diagonal of the Raman map (see Figs. 5b–5d) from the upper right to the lower left corner.

wavelength region with an increase in the content of the sp^3 phase [35] or in the degree of the sp^3 domain hybridization [36] are associated with structural disorder, which is usually accompanied by broadening of phonon bands and a decrease in their intensities in Raman spectra. Regarding the radiation of structural defects of diamond, this region of the spectrum is characteristic of the radiation of intrinsic radiation defects of diamond [38] (for example, 3H sites formed during radiation irradiation of diamond) and associated with intrinsic defects, such as vacancies or interstitial complexes [39], or complexes with an impurity in diamond crystals of types Ia and Ib (for example, 3H sites representing a neutral defect of the nitrogen–vacancy–nitrogen (NVN) type.

Usually, the hardness of diamond is estimated by the size of the imprint (diagonal dimension in the case of the Vickers indenter and the height of the imprint in the case of the Berkovich indenter) with the neglegence of the substantial concavity of its sides (see Fig. 3). In this case, the Berkovich hardness of diamond is 95–115 GPa (see Table 2). Consideration of the real area of the imprint and the change in the geometry of the indenter due to its elastic deformation leads to a sharp increase in the hardness of the diamond to 170–190 GPa. As can also be seen from Table 2, the Berkovich hardness of the (001) face of diamond of type IIb is substantially lower than the hardness of the (111) face. It should also be noted the lower hardness of diamonds of type Ib in comparison with crystals of types Ib and IIa (see Table 2). These results are in good agreement with those obtained previously [40–42] using the Knoop indenter.

There is the following problem when discussing diamond metallization: for silicon and germanium, the hardness value coincides well with the metallization pressure of these materials; for diamond, the metallization pressure (200–900 GPa, according to the ab initio calculation results [2, 43–45]) is much higher than its hardness (around 100 GPa). Possible ways to overcome this discrepancy for diamond are as follows:

— Theoretical estimates for diamond are made for the case of uniaxial or hydrostatic compression; the stress–strain state during indentation with an indenter is far from that which occurs during uniaxial compression; in particular, the shear stress values during indentation with an indenter are much higher than the shear stress values during uniaxial compression, and shear stresses substantially reduce the phase transition pressure [2];

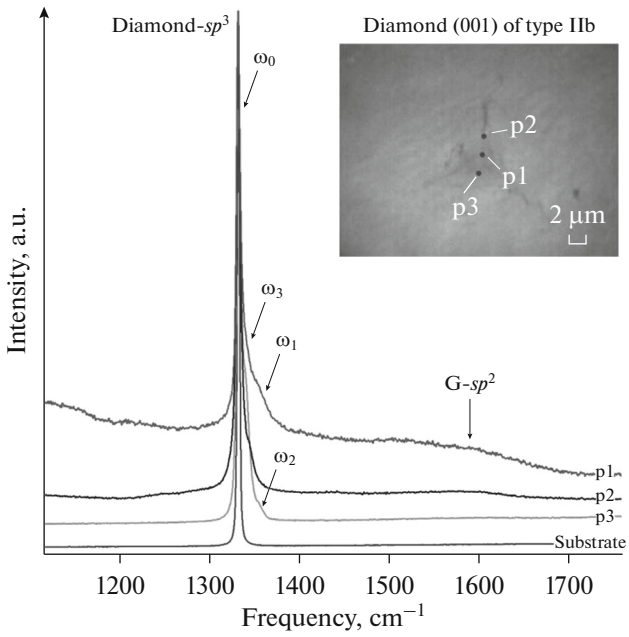

Fig. 7. Typical Raman spectra recorded in different regions of the hardness imprint on the (001) face of diamond of type IIb.

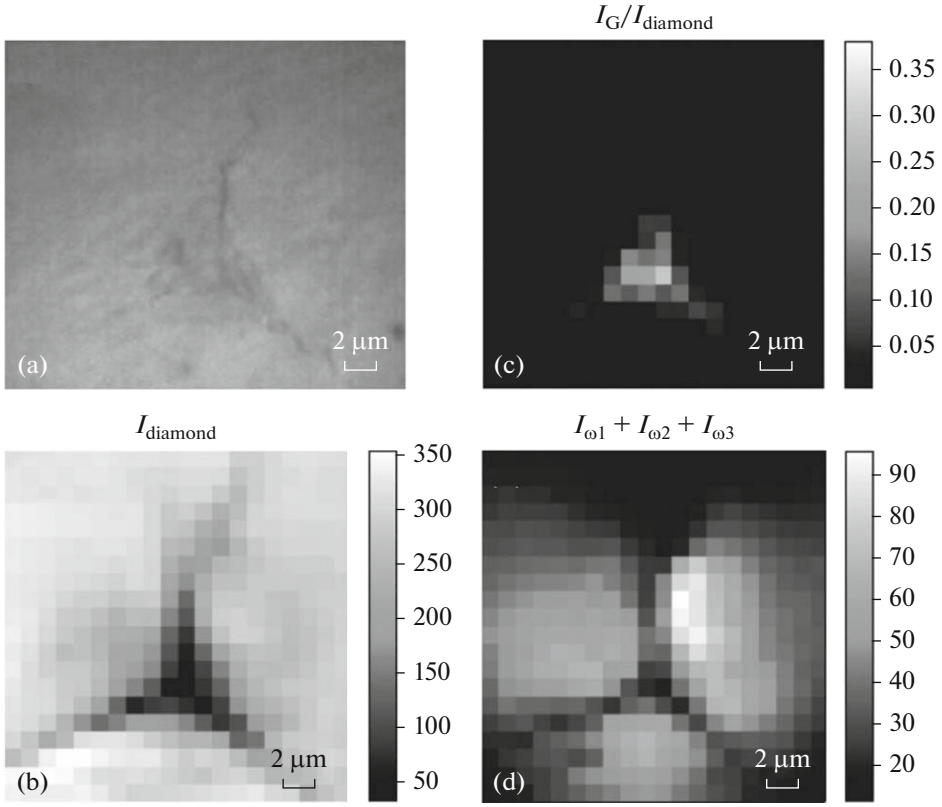

Fig. 8. (a) Optical image of the hardness test imprint on the (001) face of diamond of type IIb; (b) the distribution map of intensity $I_{diamond}$ of the Raman band of diamond at ~1333 cm^{-1}; (c) ratio $I_G/I_{diamond}$ of the mean intensity values of Raman bands of graphite and diamond; (d) total intensity $I_{\omega1} + I_{\omega2} + I_{\omega3}$ of Raman bands of strained diamond with ω_1, ω_2, and ω_3 in the range of 1340–1400 cm^{-1}.

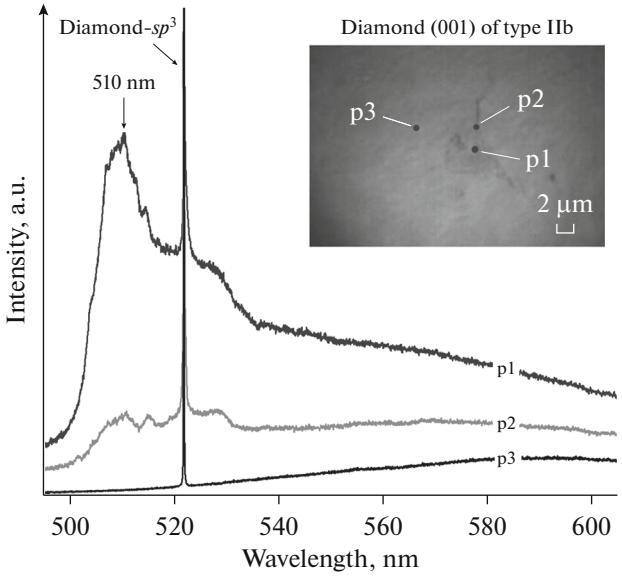

Fig. 9. Flurescence spectra recorded in different regions of the hardness test imprint on the (001) face of diamond of type IIb upon excitation by radiation with a wavelength of 488 nm.

— The hardness of diamond should be determined taking into account the concavity of the sides of the imprint and the elastic deformation of the indenter [27]; it seems that a generally accepted value of about 100 GPa for the diamond hardness is an underestated estimate; taking into account the real contact area (concavity of the sides) and the elastic deformation of the Vickers indenter gives a noticeable increase in the hardness of the (111) face of diamond to about 175–195 GPa and this agrees well with recent results of measuring the Berkovich hardness of natural diamond under a load of 1 N, which was found to be around 200 GPa [46];

— The Meyer hardness equals the average contact pressure over the imprint, but it is unevenly distributed over the imprint, namely, it is maximum in the center and decreases to zero to the imprint edge; the reason for this is apparently the fact that almost all graphite is in the central part of the imprint, which is exposed to the maximum contact pressure (Fig. 10).

CONCLUSIONS

In this study, microRaman spectroscopy is used for the first time to study the hardness imprints on the (001) face of diamond. The recording of Raman spectra of Vickers imprints on the (001) face of diamond is complicated by strong photoluminescence, so the hardness test is also performed using a Berkovich indenter, for which the deformation of the material in the region of contact is higher than for the Vickers indenter. However, the lines of the sp^2 phase of carbon in the Raman spectrum can be obtained in this case only on the surface of diamond of type IIb.

It is established that the graphitization of diamond in the imprint indented on the (001) face is weaker than in the imprint indented on the (111) face. In addition, a similar photoluminescence signal has been previously observed in films of the amorphous sp^2/sp^3-carbon material. This probably indicates that the phase transition in the imprints on the (001) face of diamond is incomplete and the mixed sp^2/sp^3 phase of amorphous carbon is formed in the hardness imprints. The likely cause of that is a lower hardness of the (001) face of diamond in comparison with the hardness of the (111) face.

It is shown that the generally accepted value of diamond hardness (around 100 GPa) is an underestated estimate. The hardness of diamond, which is measured taking into account the real area of the imprint and the change in the geometry of the indenter due to its elastic deformation, is 170–190 GPa and depends on the composition of impurities and the orientation of the sample.

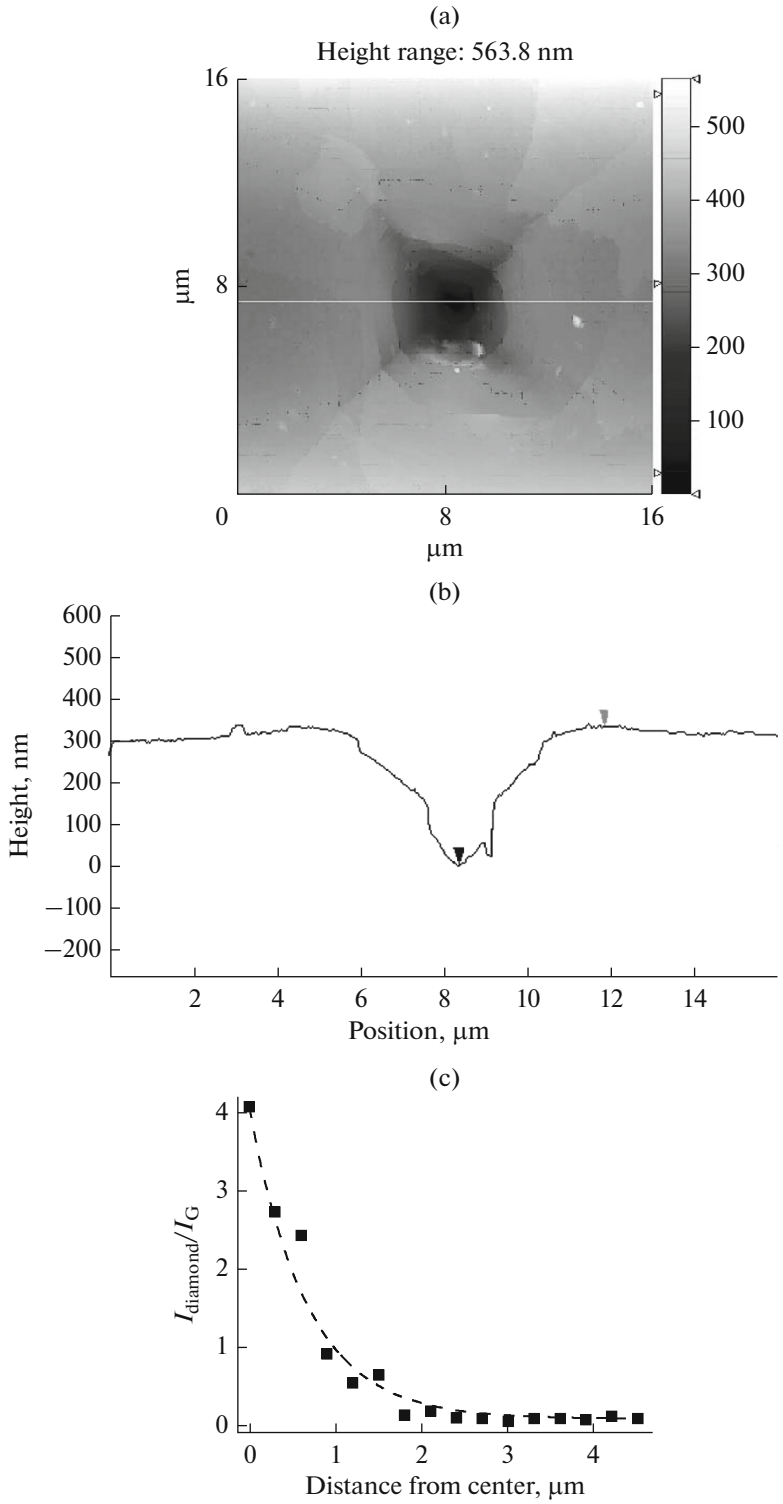

Fig. 10. (a, b) Cross section of the Vickers imprint on the (111) face of diamond of type Ib synthesized by spontaneous crystallization; (c) the distribution of graphite over the area of the imprint shown in parts (a) and (b) [27]; the main part of graphite formed during the hardness test of diamond of type Ib is concentrated in the central part of the imprint with a width of about 4 mm, which was exposed to the maximum pressure and corresponds to a sharp increase in the imprint depth in diamond (see part (b)); the size of the imprint is about twice as large as its central region enriched with graphite.

FUNDING

This study was supported by the National Research Foundation of Ukraine, project no. 2020.02/0160 entitled as "Development of New Carbon Solvents Compositions for Diamond Single Crystals Growth in the Thermodynamic

Stability Area with a Controlled Content of Nitrogen and Boron Impurities in Order to Create Conceptual Electronic Devices Construction."

CONFLICT OF INTEREST

The authors declare that they have no conflicts of ineterst.

REFERENCES

1. Gilman, J.J., Insulator-metal transitions at microindentation, *J. Mater. Res.*, 1992, vol. 7, pp. 535–538.
2. Gilman, J.J., Mechanism of shear-induced metallization, *Czech. J. Phys.*, 1995, vol. 45, pp. 913–919.
3. Besson, J.M., Itie, J.P., Polian, A., Weill, G., Masot, J.L., and Gonzalez, J., High-pressure phase transformation and phase diagram of gallium arsenide, *Phys. Rev. B*, 1991, vol. 44, pp. 4214–4234.
4. Gogotsi, Yu.G., Domnich, V., Dub, S.N., Kailer, A., and Nickel, K.G., Cyclic nanoindentation and Raman microspectroscopy study of phase transformations in semiconductors, *J. Mater. Res.*, 2000, vol. 15, pp. 871–879.
5. Gridneva, I.V., Milman, Y.V., and Trefilov, V.I., Phase transition in diamond-structure crystals during hardness measurements, *Phys. Status Solidi A*, 1972, vol. 14, pp. 177–182.
6. Pharr, G.M., Oliver, W.C., and Harding, D.S., New evidence for pressure-induced phase transformation during the indentation of silicon, *J. Mater. Res.*, 1991, vol. 6, pp. 1129–1130.
7. Kailer, A., Gogotsi, Y.G., and Nickel, K.G., Phase transformation of silicon caused by contact loading, *J. Appl. Phys.*, 1997, vol. 81, pp. 3057–3063.
8. Jang, J.-I., Lance, M.J., Wen, S., and Pharr, G.M., Evidence for nanoindentation-induced phase transformations in germanium, *Appl. Phys. Lett.*, 2005, vol. 86, 131907.
9. Domnich, V., Gogotsi, Yu., and Dub, S., Effect of phase transformations on the shape of unloading curve in the nanoindentation of silicon, *Appl. Phys. Lett.*, 2000, vol. 76, pp. 2214–2216.
10. Clarke, D.R., Kroll, M.C., Kirchner, P.D., Cool, R.F., and Hockey, B.J., Amorphization and conductivity of silicon and germanium induced by indentation, *Phys. Rev. Lett.*, 1988, vol. 60, pp. 2156–2159.
11. Bradby, J.E., Williams, J.S., Wong-Leung, J., Swain, M.V., and Munroe, P., Transmission electron microscopy observation of deformation microstructure under spherical indentation in silicon, *Appl. Phys. Lett.*, 2000, vol. 77, pp. 3749–3751.
12. Trefilov, V.I. and Mil'man, Yu.V., Specific plastic deformation of crystals with covalent bonds, *Dokl. Akad. Nauk SSSR*, 1963, vol. 153, pp. 824–827.
13. Pharr, G.M., Oliver, W.C., and Clarke, D.R., Hysteresis and discontinuity in the indentation load-displacement behavior of silicon, *Scr. Metall.*, 1989, vol. 23, pp. 1949–1952.
14. Shimomura, O., Minomura, S., Sakai, N., Asaumi, K., Tamura, K., Fukushima, J., and Endo, H., Pressure-induced semiconductor-metal transitions in amorphous Si and Ge, *Philos. Mag. A*, 1974, vol. 29, pp. 547–558.
15. Tabor, D., Phase transitions and indentation hardness of Ge and diamond, *Nature*, 1978, vol. 273, p. 406.
16. Ruoff, A.L. and Luo, H., Pressure strengthening: A possible route to obtaining 9 Mbar and metallic diamonds, *J. Appl. Phys.*, 1991, vol. 70, pp. 2066–2070.
17. Gogotsi, Yu.G., Kailer, A., and Nickel, K.G., Pressure-induced phase transformations in diamond, *J. Appl. Phys.*, 1998, vol. 84, pp. 1299–1304.
18. Gogotsi, Y.G., Kailer, A., and Nickel, K.G., Transformation of diamond to graphite, *Nature*, 1999, vol. 401, pp. 663–664.
19. Grigor'ev, O.N., The Institute for Problems of Material Sciences, National Academy of Sciences of Ukraine at Kyiv, personal communication.
20. Banerjee, A., Bernoulli, D., Zhang, H., Yuen, M.-F., Liu, J., Dong, J., Ding, F., Lu, J., Dao, M., Zhang, W., Lu, Y., and Suresh, S., Ultralarge elastic deformation of nanoscale diamond, *Science*, 2018, vol. 360, pp. 300–302.
21. Shi, Z., Dao, M., Tsymbalov, E., Shapeev, A., Lia, J., and Suresh, S., Metallization of diamond, *Proc. Natl. Acad. Sci. U. S. A.*, 2020, vol. 117, pp. 24634–24639.
22. Shi, Z., Tsymbalov, E., Dao, M., Suresh, S., Shapeev, A., and Li, J., Deep elastic strain engineering of bandgap through machine learning, *Proc. Natl. Acad. Sci. U. S. A.*, 2019, vol. 116, no. 10, pp. 4117–4122.
23. Strong, H.M. and Wentorf, R.H., The growth of large diamond crystals, *J. Naturwiss.*, 1972, vol. 59, pp. 1–7.
24. Suprun, O.M., Il'nitskaya, G.D., Kalenchuk, V.A., Zanevskii, O.A., Shevchuk, S.N., and Lysakovskii, V.V., Change of dislocations density in single crystals of various types diamonds depending on the growth temperature and rate, *Funct. Mater.*, 2016, vol. 23, no. 4, pp. 552–556.
25. Burns, R., Hansen, J., Spits, R., Burns, R.C., Sibanda, M., Welbourn, C.M., and Welch, D.L., Growth of high purity large synthetic diamond crystals, *Diamond Relat. Mater.*, 1999, vol. 8, pp. 1433–1437.

26. Novikov, N.V., Nachalna, T.A., Ivakhnenko, S.A., Zanevsky, O.A., Belousov, I.S., Malogolovets, V.G., Podzyarei, G.A., and Romanko, L.A., Properties of semiconducting diamonds grown by the temperature gradient method, *Diamond Relat. Mater.*, 2003, vol. 12, pp. 1990–1994.

27. Dub, S., Lytvyn, P., Strelchuk, V., Nikolenko, A., Stubrov, Yu., Petrusha, I., Taniguchi, T., and Ivakhnenko, S., Vickers hardness of diamond and cBN single crystals: AFM approach, *Crystals*, 2017, vol. 7, 369.

28. Burchenia, A.V., Lysakovs'kii, V.V., Gordeyev, S.O., Ivakhnenko, S.O., Kutsai, A.M., and Suprun, O.M., Calculation of the temperature distribution at the HPHT growing of diamond single crystals in cells with two growth layers, *J. Superhard Mater.*, 2017, vol. 39, no. 3, pp. 149–154.

29. Grigorovich, V.K., *Tverdost' i mikrotverdost' metallov* (Hardness and Microhardness of Metals), Moscow: Nauka, 1976.

30. Tabor, D., *Hardness of Metals*, Oxford: Clarendon, 1951.

31. Galanov, B.A., Milman, Y.V., Chugunova, S.I., and Goncharova, I.V., Investigation of mechanical properties of high-hardness materials by indentation, *J. Superhard Mater.*, 1999, vol. 21, pp. 23–35.

32. Dub, S.N., Lim, Y.Y., and Chaudhri, M.M., Nanohardness of high purity Cu (111) single crystals: The effect of indenter load and prior plastic sample strain, *J. Appl. Phys.*, 2010, vol. 107, 043510.

33. Boteler, J.M. and Gupta, Y.M., Raman spectra of shocked diamond single crystals, *Phys. Rev. B*, 2002, vol. 66, 014107.

34. Nie, A., Bu, Y., Huang, J., Shao, Y., Zhang, Y., Hu, W., Liu, J., Wang, Y., Xu, B., Liu, Z., Wang, H., Yang, W., and Tian, Y., Direct observation of room-temperature dislocation plasticity in diamond, *Matter*, 2020, vol. 2, pp. 1222–1232.

35. Papadimitriou, D., Roupakas, G., Xue, C., Topalidou, A., Panayiotatos, Y., Dimitriadis, C.A., and Logothetidis, S., Raman and photoluminescence study of magnetron sputtered amorphous carbon films, *Thin Solid Films*, 2002, vol. 414, pp. 18–24.

36. Tepliakov, N.V., Kundelev, E.V., Khavlyuk, P.D., Xiong, Y., Leonov, M.Yu., Zhu, W., Baranov, A.V., Fedorov, A.V., Rogach, A.L., and Rukhlenko, I.D., sp^2–sp^3-Hybridized atomic domains determine optical features of carbon dots, *ACS Nano*, 2019, vol. 13, pp. 10737–10744.

37. Siddique, A.B., Pramanick, A.K., Chatterjee, S., and Ray, M., Amorphous carbon dots and their remarkable ability to detect 2,4,6-trinitrophenol, *Sci. Rep.*, 2018, vol. 8, 9770.

38. Zaitsev, A.M., *Optical Properties of Diamond: A Data Handbook*, Berlin: Springer, 2001.

39. Steeds, J.W., Davis, T.J., Charles, S.J., Hayes, J.M., and Butler, J.E., 3H luminescence in electron-irradiated diamond samples and its relationship to self-interstitials, *Diamond Relat. Mater.*, 1999, vol. 8, pp. 1847–1852.

40. Sumiya, H., Super-hard diamond indenter prepared from high-purity synthetic diamond crystal, *Rev. Sci. Instrum.*, 2005, vol. 76, 026112.

41. Sumiya, H., Thermally activated deformation under Knoop indentations in super-hard directions of high-quality synthetic type-IIa diamond crystals, *Diamond Relat. Mater.*, 2006, vol. 15, pp. 1576–1579.

42. Brookes, C.A. and Brookes, E.J., Diamond in perspective: A review of mechanical properties of natural diamond, *Diamond Relat. Mater.*, 1991, vol. 1, pp. 13–17.

43. Surh, M.P., Louie, S.G., and Cohen, M.L., Band gaps of diamond under anisotropic stress, *Phys. Rev. B*, 1992, vol. 45, pp. 8239–8247.

44. van Camp, P.E., van Doren, V.E., and Devreese, J.T., Theoretical study of diamond under strong anisotropic stresses, *Solid State Commun.*, 1992, vol. 84, pp. 731–733.

45. Sichkar, S.M., Pressure-induced metallization of diamond at room temperature, *J. Superhard Mater.*, 2020, vol. 42, pp. 177–189.

46. Broadway, D.A., Johnson, B.C., Barson, M.S.J., Lillie, S.E., Dontschuk, N., McCloskey, D.J., Tsai, A., Teraji, T., Simpson, D.A., Stacey, A., McCallum, J.C., Bradby, J.E., Doherty, M.W., Hollenberg, L.C.L., and Tetienne, J.-P., Microscopic imaging of the stress tensor in diamond using in situ quantum sensors, *Nano Lett.*, 2019, vol. 19, pp. 4543–4550.

Translated by O. Kadkin